Available online at www.sciencedirect.com
SCIENCE DIRECT
Journal of Catalysis 230 (2005) 226–236
JOURNAL OF CATALYSIS
www.elsevier.com/locate/jcat

Microporous dinuclear copper(II) *trans*-1,4-cyclohexanedicarboxylate: heterogeneous oxidation catalysis with hydrogen peroxide and X-ray powder structure of peroxo copper(II) intermediate

Chika Nozaki Kato, Mari Hasegawa, Tomohiko Sato, Akira Yoshizawa, Tomonori Inoue, Wasuke Mori *

Department of Chemistry, Faculty of Science, Kanagawa University, 2946 Tsuchiya, Hiratsuka, 259-1293, Japan

Received 5 October 2004; revised 25 November 2004; accepted 25 November 2004

Abstract

A two-dimensional microporous dinuclear copper(II) *trans*-1,4-cyclohexanedicarboxylate, $[Cu_2^{II,II}(OOCC_6H_{10}COO)_2] \cdot H_2O$ (**1**), can act as a heterogeneous catalyst for selective oxidations of various alcohols with hydrogen peroxide. Complex **1** catalyzed the selective oxidations of 2-propanol, cyclohexanol, benzyl alcohol, 2-octanol, and 1-octanol with > 99% selectivities in a heterogeneous system. A green-colored active intermediate, $H_2[Cu_2^{II,II}(OOCC_6H_{10}COO)_2(O_2)] \cdot H_2O$ (**2**), observed in the reaction of **1** with a 20-fold excess H_2O_2 in acetonitrile was characterized by elemental analysis, TG/DTA, magnetic susceptibility, FT-IR, diffuse reflectance UV–vis, EPR, X-ray powder diffraction (XRPD), resonance Raman spectra, BET surface area, pore size distribution, and nitrogen occlusion measurements. The molecular structure of **2** was determined from XRPD data and refined by the Rietveld method. The microporous structure of **2** was constructed by intramolecular bridging of μ-1,2-*trans* Cu–OO–Cu species between two-dimensional $[Cu_2(O_2CC_6H_{10}CO_2)]$ layers. The complex **2** was the first example of the microporous copper(II) peroxo complex for heterogeneous oxidation catalysis.

Keywords: Copper carboxylate polymer complex; Microporous materials; Oxidation of alcohol with hydrogen peroxide; Copper peroxo intermediate; Gas adsorption property

1. Introduction

The heterogeneous oxidation catalysis of alcohols with an environmentally suitable oxidant, hydrogen peroxide (H_2O_2), is quite an interesting objective for both the academic and industrial fields [1–3]. Among the newer heterogeneous oxidation catalysts attracting interest are copper-containing porous and nonporous materials, such as Cu^{2+}-phthalocyanine incorporated inside Y faujasite and MCM-41 [4], Cu-HMS [5], Cu^{2+}-substituted MCM-41 [6], zeolite-encapsulated Cu^{2+}-salens [7], Cu^{2+}/X and Y zeolite [8], $Cu(OH)_2/SiO_2$ [9], and *cis*-bisglycianato copper(II)/1,6-naphthalenediol oligomer [10], which have been shown to be active for selective oxidations of a variety of organic compounds in the presence of H_2O_2 or organic peroxide.

For the homogeneous oxidations catalyzed by biomimetic dicopper complexes with dioxygen and H_2O_2 as oxidants, a large number of dinuclear copper complexes have recently been reported as model compounds for the active sites of type 3 copper hemocyanin and tyrosinase [11–20]. Various biomimetic copper complexes have been used as homogeneous oxidation catalysts, and various peroxo copper intermediates have been studied to investigate the oxygen-transfer mechanisms of copper proteins [15–18,20]; however, the studies on the heterogeneous catalytic activities of single copper active sites and the nature of oxidizing species are still particularly challenging, given the difficulties inherent in characterizing active sites under reaction conditions

* Corresponding author.
E-mail address: wmori@chem.kanagawa-u.ac.jp (W. Mori).

0021-9517/$ – see front matter
doi:10.1016/j.jcat.2004.11.032

[4–10]. Despite the advantage of synthesizing active and selective catalytic centers in heterogeneous catalysis, none of the copper-containing heterogeneous catalysts mentioned in this paper have been shown to oxidize a wide variety of alcohols with H_2O_2.

Microporous organic–inorganic hybrid coordination polymers have attracted much attention because of their molecular adsorption, including not only gas molecules but also organic molecules [21–41], ion-exchange, and catalytic activities [30–33]. Of all these efficient porous materials, we have studied in particular the synthesis of transition-metal carboxylate coordination polymers, such as dicarboxylates of copper [21,22,34–37], molybdenum [38], and ruthenium [39,40], which are capable of occluding large amounts of gases such as N_2, Ar, O_2, CH_4, and Xe. Not only are their uniform linear micropores constructed by the stacking or bonding of two-dimensional lattices of dinuclear transition metal carboxylates; single-site mono- and dinuclear transition metal centers in uniform linear pores are also important points for the use of these metal carboxylates as heterogeneous catalysts. In the progress of these studies, we have especially focused on the use of one of the dinuclear copper(II) carboxylates, copper(II) *trans*-1,4-cyclohexanedicarboxylate (**1**) [34–37], as a heterogeneous oxidation catalyst because of its high stability toward oxidants such as H_2O_2. We have also investigated the structure and nature of the oxidizing copper intermediates in uniform micropores because they would be the keys to the development of new heterogeneous oxidation catalysts.

In this paper we report the heterogeneous oxidations of various alcohols catalyzed by complex **1** with H_2O_2. A microporous peroxo copper(II) intermediate was isolated and characterized by elemental analysis, FT-IR, TG/DTA, magnetic susceptibility, EPR, X-ray powder diffraction (XRPD), resonance Raman, diffuse reflectance (DR) UV–vis, BET surface area, pore size, and gas occlusion measurements. We also investigated a NMR tube reaction of 2-propanol to form acetone by the oxidizing intermediates in the absence of H_2O_2 to determine whether the obtained copper peroxo complex was a real active species for the heterogeneous oxidation catalysis.

2. Experimental

2.1. Materials

The following chemicals were used as received: 2-propanol, cyclohexanol, benzyl alcohol, 2-octanol, 1-octanol, acetonitrile, and 30% aqueous H_2O_2 solution (quantitative analysis grade; Wako). Synthesis and characterization results for copper(II) *trans*-1,4-cyclohexanedicarboxylate, $[Cu_2^{II,II}(OOCC_6H_{10}COO)_2]\cdot H_2O$ (**1**), were reported in our previous paper [34–37]. The obtained complex **1** was dried at 100 °C under vacuum for 2 h.

2.2. Instrumentation/analytical procedures

Elemental analyses were performed on a Perkin–Elmer 2400 CHNS Elemental Analyzer II at Kanagawa University. Infrared spectra were recorded on a Jasco 300 FT-IR spectrometer in KBr disks at room temperature. Thermogravimetric (TG) and differential thermal analyses (DTA) were acquired with a Rigaku TG8101D and TAS 300 data-processing system. TG/DTA measurements were performed in air with a temperature ramp of 4 °C/min between 20 and 500 °C. Diffuse reflectance (DR) UV–vis spectra were recorded on a Jasco V-560 spectrophotometer equipped with a Jasco diffuse-reflectance attachment. Specific surface areas were measured by the BET method with an ASAP 2010 (Shimadzu). The pore size diameter was calculated by the Horvath–Kawazoe (HK) method [42]. X-band EPR spectra were recorded on a JEOL JES-RE Series EPR spectrometer at room temperature. Resonance Raman spectra were recorded on a reflex Raman microscope (Renishaw) with a LD:YAG laser as the source of 532-nm radiation within 3 mW. A solid sample was grounded and irradiated. The temperature dependence of magnetic susceptibility was measured with a SQUID magnetometer (Quantum Design; MPMS-5S) in the temperature range of 2–300 K. The temperature dependence of the amount of adsorbed nitrogen was measured with a Cahn 1000 electric balance at 20 Torr in a temperature range of 77.5–270 K [21–23]. ^{1}H NMR in CD_3CN solution spectra was recorded at 399.65 MHz on a JEOL JNM-EX 400 FT-NMR spectrometer with a JEOL EX-400 NMR data-processing system. Chemical shifts, δ, were referenced to TMS. XRPD was performed on a Bruker M18XHF diffractometer (Cu-K_α, $\lambda = 0.15406$ nm, 35.0 kV, 200.0 mA) at room temperature. Intensity data were collected by step-counting methods (step 0.01° and sampling time 1.0 s) in the range of 5°–60° angles.

2.3. Synthesis of $H_2[Cu_2^{II,II}(OOCC_6H_{10}COO)_2(O_2)]\cdot H_2O$ (**2**)

The dinuclear copper(II) peroxo complex was prepared as follows: 30% H_2O_2 aqueous solution (648.8 µL, 8.24 mmol) was added to a suspension of complex **1** (100 mg, 206 µmol) in acetonitrile (10 mL) at room temperature. After addition of H_2O_2, the color of the reaction suspension changed from blue to green for a few minutes. Here, the pH of this suspension was changed from neutral to acidic by the addition of H_2O_2, suggesting that a heterolytic H–OOH bond cleavage in **1** had occurred. The green-colored precipitate was collected after 4 h of stirring and was washed with acetonitrile (50 mL × 3) and methanol (50 mL × 3). The green-colored precipitate obtained was dried under vacuum at room temperature for 2 h. [Yield: 94.5 mg (87.8%). Elemental analysis: found: C, 37.00; H, 4.66%; calcd. for $C_{16}H_{24}O_{11}Cu_2 = H_2[Cu_2(C_8H_{10}O_4)_2(O_2)]\cdot H_2O$: C, 37.07; H, 4.47%. TG/DTA data: 5.35% weight loss was observed below 136.4 °C with an exothermic peak at 132.8 °C, sug-

gesting the decomposition of $Cu(H_2O_2)$ species (6.5%). Decomposition of organic ligand began around 245 °C (54.26% weight loss) with an exothermic peak at 242.7 °C. IR (KBr disks): 1594s, 1511w, 1423s, 1373w, 1332w, 1297m, 1222w, 1045w, 929w, 784m, 767m, 727w, 526m cm^{-1}. BET surface area: 328.4 m^2/g. Pore size diameter: 4.9 Å. Maximum amount of nitrogen occluded by **2**: 1.09 mol/mol of copper. DR–UV spectrum: λ_{max} 260, 385, 665 nm. EPR spectra: EPR silent state. Raman spectrum: 805 [ν(O–O)] cm^{-1}.]

2.4. Structure solution and refinements of $[Cu_2^{II,II}(OOCC_6H_{10}COO)_2] \cdot H_2O$ (1) and $H_2[Cu_2^{II,II}(OOCC_6H_{10}COO)_2(O_2)] \cdot H_2O$ (2)

The low-angle powder diffraction patterns of complexes **1** and **2** were indexed with the TREOR 90 and DICVOL 91 programs, which suggested a primitive triclinic cell with the following unit-cell parameters: for complex **1**, $a = 10.552(9)$, $b = 10.351(7)$, $c = 5.103(6)$ Å, $\alpha = 72.317(5)$, $\beta = 90.844(1)$, $\gamma = 101.576(5)°$; for complex **2**, $a = 10.818(7)$, $b = 10.238(1)$, $c = 7.102(9)$ Å, $\alpha = 74.836(1)$, $\beta = 101.942(6)$, $\gamma = 106.725(7)°$. These structures were refined by the Rietveld method with a DBWS program. Powder diffraction patterns were calculated for this model in the triclinic space group $P1$ and with the use of the unit-cell parameters refined by a least-squares procedure described above. Data were evaluated in the angle ranges of 5°–60° 2θ.

2.5. Catalytic oxidations

A sample of the catalyst (100 mg, 206 μmol) was added to a Schlenck tube under an Ar atmosphere. The substrates (2-propanol, cyclohexanol, benzyl alcohol, 2-octanol, 1-octanol) (6.4–13.1 mmol) and acetonitrile (10 mL) were added with a micropipette. The mixture was allowed to equilibrate at a reaction temperature of 20 °C for 10 min. Thirty percent aqueous H_2O_2 (9.71–48.5 mmol, 23–113-fold excess of copper) was added with a micropipette to the rapidly stirred solution. The samplings were carried out after 10 and 30 min and 1, 2, 3, 24, 48, 72, 96, 144, and 168 h. Before the samplings, the solid catalyst was washed with excess methanol to remove the oxidative products in the cavities of the catalyst into the reaction solution. The reaction solution was analyzed by GC (FID, SE-30 glass column and DB-WAX capillary column (0.53 mm o.d., 15 m)) and HPLC (Shim-pack VP-ODS 150 mm L. × 4.6 mm i.d.), and assignments were made by comparison with authentic samples analyzed under the same conditions.

3. Results and discussion

3.1. Catalytic oxidations

Complex **1** was used as a heterogeneous catalyst for the oxidations of 2-propanol, cyclohexanol, benzylalcohol, 1-octanol, and 2-octanol with H_2O_2 at 20 °C, as shown in Eq. (1). The catalytic activities (turnover frequencies, conversions, and selectivities of oxidative products) and their catalytic behavior were influenced by the concentrations of H_2O_2, that is, for all oxidation reactions with varying concentrations (less than 46-fold and more than 69-fold excess) of H_2O_2, the color of complex **1** changed from blue to green and brown. The green and brown colors persisted for 2 days and 3 weeks, respectively, and then disappeared. The catalytic oxidation results for various concentrations of H_2O_2 are summarized in Table 1.

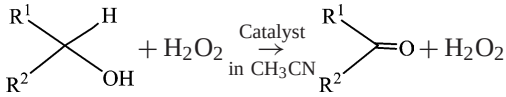

(1)

R^1 = aryll, alkyl; R^2 = H, alkyl

For the oxidation of 2-propanol with two different concentrations of H_2O_2 (23- and 113-fold excess of copper atom), the conversions leading to formation of acetone were observed to be highly selective (100 out to 17% (after 1 h) and 56% (after 3 h) conversions of 2-propanol, respectively) and to occur with turnover frequencies (TOF = (mol of products)/((mol of complex) s)) of 1.6×10^{-3} s^{-1} and 5.8×10^{-3} s^{-1} (calculated after a reaction time of 1 h), respectively. No induction period was observed for reactions involving both concentrations of H_2O_2 ($\geqslant$ 10 min). When the green and brown colors disappeared, the reaction stopped, suggesting that the green and brown species were active intermediates for oxidation catalysis. The organic carboxylate ligands of other microporous dinuclear copper(II) carboxylates, for example, copper(II) telephthalate and copper(II) fumarate, were decomposed to H_2O_2 and other biomimetic copper complexes [15]. In contrast, the FT-IR spectrum of complex **1** after catalysis showed 13 bands at 1594s, 1511w, 1423s, 1373w, 1332w, 1297m, 1222w, 1045w, 929w, 784m, 767m, 727w, 526m cm^{-1}, which were consistent with as-prepared complex **1** (1598s, 1513w, 1425s, 1371w, 1334w, 1295m, 1220w, 1047w, 927w, 782m, 728w, 530m cm^{-1}), except for a band at 767 cm^{-1}, which that could be assigned to ν(C–H) of the cyclohexane ring [43], which might be due to the rotation of the cyclohexane ring caused by the coordination of hydrogen peroxide and/or the alcohol molecule to the copper center. Complex **1** was also characterized after oxidation catalysis by elemental analysis, UV–vis, XRPD, BET surface area, and pore size distribution measurements: the XRPD pattern showed 14 lines at $2\theta(°) = 8.56, 9.20, 10.88, 14.13, 17.24, 18.55, 19.25, 20.10, 21.90, 22.66, 23.92, 25.22, 26.08, 28.63$ with relative intensities of 100, 75, 9, 4, 23, 10, 13, 10, 2, 6, 7, 6, 7, 5, respectively, in the 2°–30° angles. The BET surface was 301.2 m^2/g (the pore size diameter was 5.1 Å). The DR–UV spectrum showed three bands at 261, 375, and 660 nm. (Elemental analysis: found: C, 38.33; H, 4.97%, calcd. for $C_{16}H_{24}O_{10}Cu_2 = [Cu_2(C_8H_{10}O_4)_2] \cdot 2H_2O$: C, 38.17; H, 4.80%.) These results were consistent with those for as-

Table 1
Oxidation of alcohols with H_2O_2 catalyzed by copper(II) *trans*-1,4-cyclohexanedicarboxylate (**1**) at 20 °C

Entry	Substrate (mmol)	Selectivity[a] (%)	TOF[b] (s^{-1})	Conversion (%) (TON) [reaction time]
1	2-Propanol (13.1)	Acetone (> 99)	1.6×10^{-3}	17.1 (11) [1 h]
2[c]	2-Propanol (13.1)	Acetone (> 99)	5.8×10^{-3}	55.6 (35) [3 h]
3[d]	Cyclohexanol (9.5)	Cyclohexanone (> 99)	1.1×10^{-4}	14.3 (6.5) [168 h]
4[c]	Cyclohexanol (9.5)	Cyclohexanone (> 99)	1.6×10^{-4}	19.8 (9.1) [168 h]
5	Benzylalcohol (9.7)	Benzaldehyde (> 99)	7.0×10^{-4}	16.7 (7.8) [144 h]
6[c]	Benzylalcohol (9.7)	Benzaldehyde (> 99)	1.5×10^{-3}	25.8 (12) [144 h]
7	1-Octanol (6.4)	Octylaldehyde (> 99)	1.1×10^{-4}	10.8 (3.4) [168 h]
8[c]	1-Octanol (6.4)	Octylaldehyde (> 99)	1.6×10^{-4}	13.2 (4.1) [168 h]

Reaction conditions: catalyst 206 μmol, substrate 6.4–13.1 mmol, 30% H_2O_2 9.7 mmol (23-fold excess), CH_3CN 10 ml.
[a] After 1 h.
[b] TOF = turnover number (TON)/s after 1 h.
[c] H_2O_2 (48.5 mmol, 113-fold excess) was used.
[d] H_2O_2 (19.4 mmol, 46-fold excess) was used.

prepared complex **1**, suggesting that the structure of complex **1** was maintained after oxidation catalysis with H_2O_2.

To determine whether the active species leached into the solution during a typical catalytic reaction, the mixture of complex **1** and a 23-fold excess of H_2O_2 in acetonitrile was stirred for 3 days at 20 °C. The mixture was then filtered via a Büchner funnel (Whatman No. 2), and the filtrate was treated with 2-propanol at 20 °C. The samples of this reaction mixture taken after 1, 2, and 3 h contained no oxidation products, indicating that the observed catalysis was heterogeneous. Using the solid after filtration as a catalyst, we carried out the oxidation of 2-propanol with a 23-fold excess of H_2O_2 at 20 °C. The TOF of 1.2×10^{-3} s^{-1} was similar to that found for the first use (1.6×10^{-3} s^{-1}). In addition, no copper species was detected in the filtrate (< 0.02 ppm). These results indicated that leaching of a catalytically active copper species in the solution was negligible.

Complex **1** was observed to catalyze the oxidation of cyclohexanol to cyclohexanone (100% selectivity) with two different concentrations of H_2O_2 (46-fold and 113-fold excess of copper atoms). Furthermore, no induction period was observed for the reactions with either concentration of H_2O_2 (⩾ 10 min). TOFs were 1.1×10^{-4} s^{-1} and 1.5×10^{-4} s^{-1} after 1 h, and conversions of 14.3 and 19.8% were achieved with the two different concentrations of hydrogen peroxide, respectively, after 168 h. Although complex **1** can adsorb relatively large organic molecules, such as *o*-xylene (0.3 mol/mol of copper), *m*-xylene (0.4 mol/mol of copper), and *p*-xylene (0.3 mol/mol of copper) [44], the observed TOFs were lower than those of 2-propanol oxidation with 23- and 113-fold excess H_2O_2 because it might be easier for 2-propanol to enter a micropore than it would for cyclohexanol and/or for acetone to exit a micropore than it would for cyclohexanone. As a control experiment, nonporous $Cu(OH)_2$ was used as a solid catalyst for cyclohexanol oxidation with a 46-fold excess of H_2O_2, but the activity was low (TON < 1 after 144 h).

Complex **1** was also observed to catalyze the oxidation of benzyl alcohol to benzaldehyde (100% selectivity) with two different concentrations of H_2O_2 (46- and 113-fold excess of copper atoms). Furthermore, no induction period was observed for the reactions involving both concentrations of H_2O_2 (⩾ 10 min). TOFs were 7.0×10^{-4} s^{-1} and 1.5×10^{-3} s^{-1} after 1 h, and conversions reached 16.7 and 25.8%, respectively, after 144 h. For comparison, the observed TOF, 1.5×10^{-3} s^{-1}, was higher than 8.9×10^{-4} s^{-1} for *cis*-bisglycinato copper(II)/1,6-naphthalenediol oligomer [10].

Complex **1** can oxidize not only secondary alcohols and benzylic alcohol, but also primary alcohols with high selectivities and conversions. The oxidation of 1-octanol to octyl aldehyde with both concentrations of H_2O_2 (23- and 113-fold excess of hydrogen peroxide) proceeded with high selectivity (ca. 100%) over 168 h. Whereas most oxidations occur more rapidly with secondary alcohol than with primary alcohol, the oxidations via the formation of metal-alcoholate intermediate lead to selective oxidation of primary hydroxyl groups [45–48]. The TOFs (1.1×10^{-4} s^{-1} and 1.6×10^{-4} s^{-1} after 1 h) for 1-octanol oxidation were faster than those for 2-octanol oxidation (4.1×10^{-5} s^{-1} and 5.5×10^{-5} s^{-1} after 1 h) with > 99% selectivity of 2-octanone under the same reaction conditions, and the conversions (10.8 and 13.2% after 168 h) were also higher than those for 2-octanol oxidation (2–3% after 168 h), suggesting that a copper–alcoholate intermediate was also formed. Thus, these results suggested that both copper–alcoholate species and copper–peroxo species were formed as intermediates during the course of reaction.

3.2. Synthesis, structure, and compositional characterization of microporous peroxo copper(II) complex, $H_2[Cu_2^{II,II}(OOCC_6H_{10}COO)_2(O_2)] \cdot H_2O$ (2)

As mentioned above, the green- and brown-colored intermediates were observed with the addition of different concentrations (less than 46-fold and more than 69-fold excess) of H_2O_2, respectively, in the studies of catalytic oxidations. Here, the green-colored intermediate was isolated and characterized by elemental analysis, FT-IR, TG/DTA, magnetic

Table 2
Crystallographic data for complexes **1** and **2**

	1	**2**
Empirical formula	$H_{20}C_{16}O_8Cu_2$	$H_{20}C_{16}O_{10}Cu_2$
Formula weight	467.422	499.42
Crystal color	Blue powder	Green powder
Crystal system	Triclinic	Triclinic
Space group	$P1$ (#1)	$P1$ (#1)
Lattice parameters	$a = 10.552(9)$ Å	$a = 10.818(7)$ Å
	$b = 10.351(7)$ Å	$b = 10.238(1)$ Å
	$c = 5.103(6)$ Å	$c = 7.102(9)$ Å
	$\alpha = 72.317(5)°$	$\alpha = 74.836(1)°$
	$\beta = 90.844(1)°$	$\beta = 101.942(6)°$
	$\gamma = 101.576(5)°$	$\gamma = 106.725(7)°$
	$V = 519.53(4)$ Å^3	$V = 719.63(6)$ Å^3
Z, calculated density	1, 1.6614 g/cm^3	1, 1.1524 g/cm^3
Residuals; R-p, R-wp	11.79%; 15.44%	10.36%; 13.81%

susceptibility, ESR, DR–uv, XRPD, resonance Raman, BET surface area, pore size distribution, and gas occlusion measurements. The green color of the copper intermediate did not appear until the 20-fold excess of H_2O_2 was added. Brown species could not be obtained as a pure solid.

The solid green oxidizing copper(II) intermediate, $H_2[Cu_2^{II,II}(OOCC_6H_{10}COO)_2(O_2)] \cdot H_2O$ (**2**), was obtained in 87.8% (94.5 mg scale) yield, which was prepared by the reaction of complex **1** in acetonitrile suspension with a 20-fold excess of H_2O_2, followed by washing with excess amounts of acetonitrile and methanol, and then by drying under vacuum for 2 h at 25 °C. According to elemental analysis results, the pure complex **2** could not be obtained with less than a 20-fold excess of hydrogen peroxide, which might be due to the hydrophobicity in the micropore of complex **1**. The formation of **2** can be shown in an ionic balance equation:

$$\left[Cu_2^{II,II}(OOCC_6H_{10}COO)_2\right] + H_2O_2 \rightarrow \left[Cu_2^{II,II}(OOCC_6H_{10}COO)_2(O_2)\right]^{2-} + 2H^+ \quad (2)$$

The XPRD patterns of complexes **1** and **2** were recorded, and the crystal structures were solved and refined by the Rietveld method (see the Experimental section). The final R-p and R-wp agreement factors, together with data collection details and analyses for complexes **1** and **2**, are given in Table 2. The final Rietveld plots are shown in Figs. 1a and b. The XRPD pattern of complex **1** showed 15 lines at $2\theta(°) = 8.53, 9.12, 11.16, 17.13, 17.43, 17.69, 18.30, 19.28, 20.11, 21.57, 22.71, 24.02, 25.54, 25.79, 26.03$ with relative intensities of 100, 54, 5, 17, 6, 5, 6, 8, 6, 2, 3, 3, 4, 4, 3, respectively, in the 2°–30° angles. For complex **2**, 10 lines were observed at $2\theta(°) = 8.50, 9.09, 10.82, 17.10, 18.24, 19.27, 20.06, 22.71, 24.01, 26.03$ with the relative intensities of 100, 69, 9, 19, 10, 13, 11, 6, 7, 8, respectively. Bond lengths and angles are listed in Table 3, and final fractional coordinates are reported in Tables S1 and S2, provided as supporting information.

The molecular structure of **1** (Fig. 2a) was isomorphous to several [Cu_2^{II}(μ-carboxylate)] complexes, the crystal structures of which have previously been reported [49]. Figs. 3a–c show the perspective views of the stacking complex **1** along with the a, b, and c axes, respectively. The intramolecular coordination of an oxygen atom of carboxylate ligand to the vacant site of copper atom caused the stacking of the two-dimensional [$Cu_2(O_2CC_6H_{10}CO_2)$] layers to form three-dimensional lattice structures. In contrast, X-ray structure analysis of complex **2** (Fig. 2b) revealed that the microporous structure of complex **2** was constructed by the bridging of the μ-1,2-*trans* Cu(1)–OO–Cu(2)′ species between two-dimensional [$Cu_2(O_2CC_6H_{10}CO_2)$] layers as shown in Figs. 4a and b. The Cu(1)–O(9) and Cu(2)′–O(10) distances were 1.877(2) Å and 1.879(1) Å, respectively, which were quite similar to those of μ-1,2-*trans*-copper(II) peroxo complex determined by X-ray crystal analysis (1.852 Å) [50] and slightly shorter than those of reported side-on copper(II) peroxo complexes (1.892–1.941 Å) [18], but much longer than those of copper(III) peroxo complexes (ca. 1.80 Å) [19,51]. The intermolecular Cu(1)···Cu(2)′ separation stretched to 4.572(4) Å, which was much longer than the Cu(1)···Cu(2)′ separation (2.992(6) Å) for complex **1**, because of the insertion of intra-peroxide ligand in the two-dimensional layers. The intermolecular Cu(1)···Cu(2) separation of complex **2** is 2.632(2) Å, which was similar to that of complex **1** (2.642(9) Å), suggesting that intramolecular Cu(1)···Cu(2)

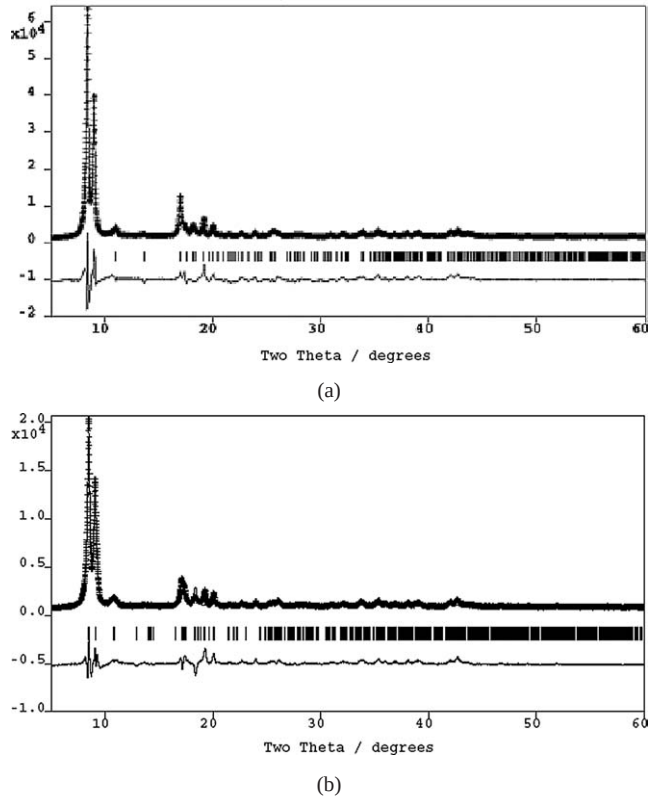

Fig. 1. Observed (+++) and calculated (—) powder X-ray diffraction profiles for the Rietveld refinement of complexes **1** (a) and **2** (b). The bottom curve is the difference plot on the same intensity. The tic marks are the calculated 2θ angles for Bragg peaks.

Table 3
Selected bond distances (Å) and angles (°) around the copper(II) centers for complexes **1** and **2**

Complex **1**					
Cu(1)···Cu(2)	2.632(2)	O(1)–Cu(1)–O(5)	169.0(4)	O(4)–Cu(2)–O(6)	89.2(6)
Cu(1)–O(1)	2.059(1)	O(3)–Cu(1)–O(7)	168.3(8)	O(6)–Cu(2)–O(8)	88.0(6)
Cu(1)–O(3)	1.984(2)	O(2)–Cu(2)–O(6)	170.7(9)	Cu(2)–Cu(1)–O(1)	84.3(9)
Cu(1)–O(5)	2.059(2)	O(4)–Cu(2)–O(8)	167.2(4)	Cu(2)–Cu(1)–O(3)	84.2(9)
Cu(1)–O(7)	1.985(9)	O(1)–Cu(1)–O(3)	88.2(9)	Cu(2)–Cu(1)–O(5)	85.4(8)
Cu(2)–O(2)	2.051(8)	O(1)–Cu(1)–O(7)	89.3(6)	Cu(2)–Cu(1)–O(7)	84.2(8)
Cu(2)–O(4)	1.985(4)	O(3)–Cu(1)–O(5)	87.2(8)	Cu(1)–Cu(2)–O(2)	86.3(8)
Cu(2)–O(6)	2.042(2)	O(5)–Cu(1)–O(7)	93.3(1)	Cu(1)–Cu(2)–O(4)	83.7(3)
Cu(2)–O(8)	1.988(8)	O(2)–Cu(2)–O(4)	93.6(4)	Cu(1)–Cu(2)–O(6)	85.2(1)
Cu(1)···Cu(2)′	2.992(6)	O(2)–Cu(2)–O(8)	87.4(7)	Cu(1)–Cu(2)–O(8)	83.6(5)
Complex **2**					
Cu(1)···Cu(2)	2.642(9)	O(1)–Cu(1)–O(5)	169.6(9)	Cu(1)–Cu(2)–O(2)	85.7(2)
Cu(1)–O(1)	1.987(2)	O(3)–Cu(1)–O(7)	171.6(5)	Cu(1)–Cu(2)–O(4)	86.0(2)
Cu(1)–O(3)	2.023(9)	O(2)–Cu(2)–O(6)	171.6(7)	Cu(1)–Cu(2)–O(6)	86.4(3)
Cu(1)–O(5)	1.982(9)	O(4)–Cu(2)–O(8)	171.4(3)	Cu(1)–Cu(2)–O(8)	86.0(1)
Cu(1)–O(7)	1.998(9)	O(1)–Cu(1)–O(3)	90.1(9)	O(1)–Cu(1)–O(9)	89.6(3)
Cu(2)–O(2)	1.983(7)	O(1)–Cu(1)–O(7)	92.4(5)	O(3)–Cu(1)–O(9)	101.0(1)
Cu(2)–O(4)	1.993(1)	O(3)–Cu(1)–O(5)	86.1(5)	O(5)–Cu(1)–O(9)	100.6(1)
Cu(2)–O(6)	2.024(1)	O(5)–Cu(1)–O(7)	89.9(7)	O(7)–Cu(1)–O(9)	87.0(6)
Cu(2)–O(8)	1.988(1)	O(2)–Cu(2)–O(4)	90.0(3)	Cu(2)–Cu(1)–O(9)	171.4(5)
Cu(1)–O(9)	1.877(2)	O(2)–Cu(2)–O(8)	86.2(3)	Cu(1)–O(9)–O(10)	125.1(2)
O(9)–O(10)	1.230(9)	O(4)–Cu(2)–O(6)	92.5(8)	O(9)–O(10)–Cu(2)′	124.7(7)
Cu(2)′–O(10)	1.879(1)	O(6)–Cu(2)–O(8)	90.2(7)	O(10)–Cu(2)′–O(2)′	99.7(3)
Cu(1)···Cu(2)′	4.572(4)	Cu(2)–Cu(1)–O(1)	85.6(2)	O(10)–Cu(2)′–O(4)′	88.2(3)
		Cu(2)–Cu(1)–O(3)	86.1(4)	O(10)–Cu(2)′–O(6)′	88.4(9)
		Cu(2)–Cu(1)–O(5)	84.4(4)	O(10)–Cu(2)′–O(8)′	100.0(9)
		Cu(2)–Cu(1)–O(7)	86.1(4)	O(10)′–Cu(2)–Cu(1)	172.1(9)

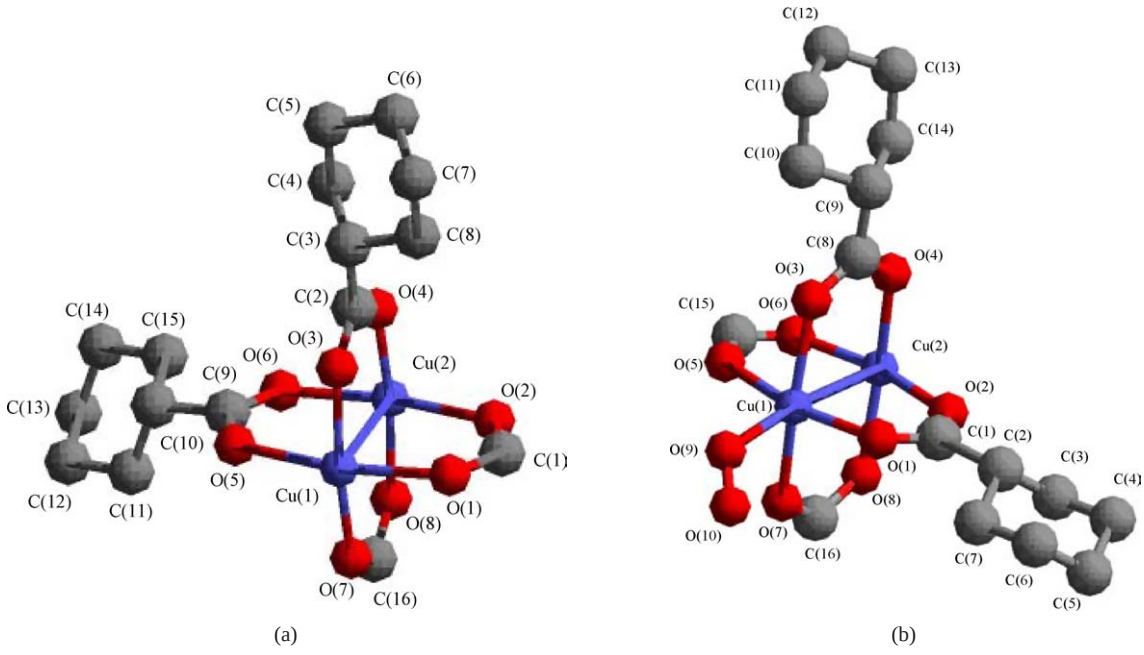

Fig. 2. Molecular structures and atom labeling scheme showing only the Cu^{2+} coordination environment as formed in complexes (a) **1** and (b) **2**.

interaction was not affected by the coordination of peroxo ligand between two-dimensional $[Cu_2(O_2CC_6H_{10}CO_2)]$ layers. The size of the micropore structure for complex **1** was altered slightly by the bridging of μ-1,2-*trans*-Cu(1)–OO–Cu(2)′ intramolecular bonding as shown in Figs. 3c and 4c. The space formed by bridging of peroxo ligand between layers for complex **2** can make possible the rotation of the cyclohexane ring of complex **1**. To our knowledge, complex **2** is the first example of the microporous copper(II) peroxo complex.

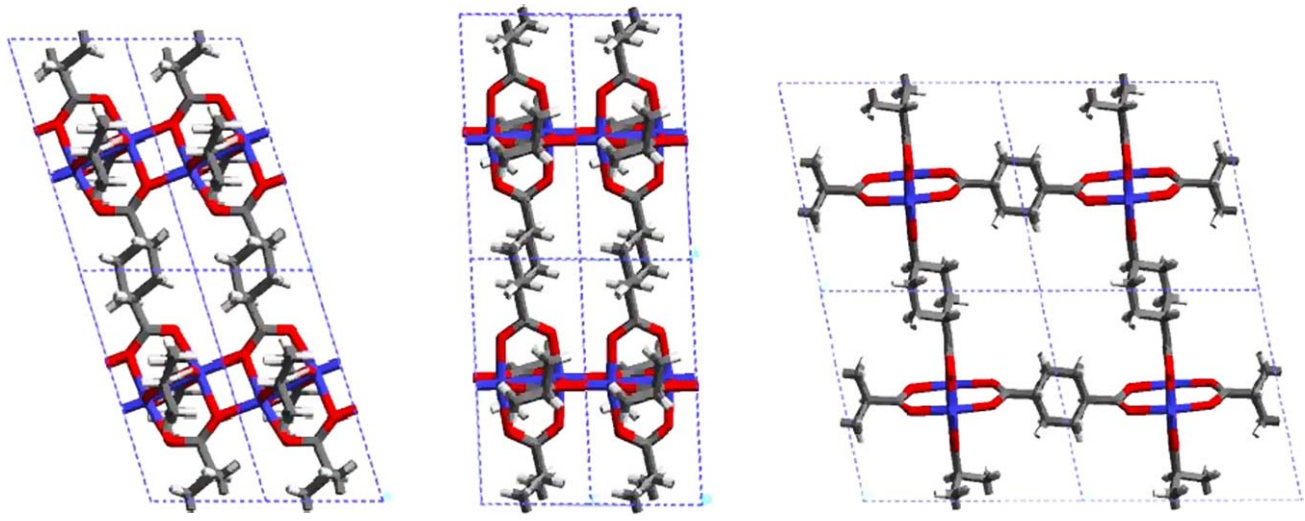

(a) (b) (c)

Fig. 3. Unit-cell packing of complex **1** viewed along the (a) *a*, (b) *b*, and (c) *c* axes.

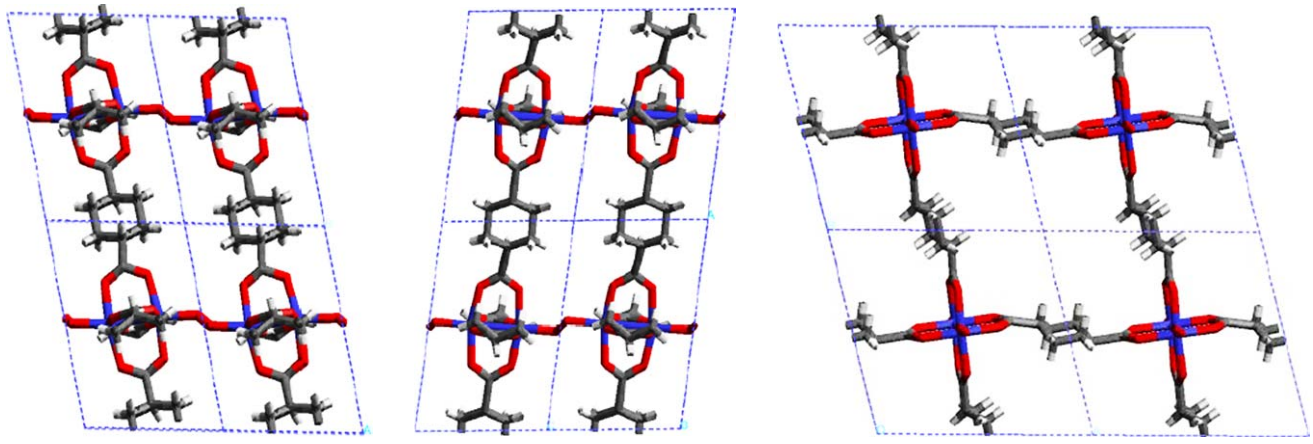

(a) (b) (c)

Fig. 4. Unit-cell packing of complex **2** viewed along the (a) *a*, (b) *b*, and (c) *c* axes.

Other characterization results for complex **2** were consistent with the result of Rietveld analysis. The C and H elemental analysis data were consistent with a composition of $H_2[Cu_2^{II,II}(OOCC_6H_{10}COO)_2(O_2)] \cdot H_2O$. The pH of complex **1** was changed from neutral to acidic with the addition of H_2O_2, also suggesting that the Cu–OO–Cu species was formed by a heterolytic H–OOH bond cleavage in complex **1**. The TG/DTA measurement for complex **2** (as shown in Fig. 5b), performed under atmospheric conditions, showed a weight loss of 5.35% with an exthothermic peak at 132.8 °C, which corresponded to the decomposition of peroxo ligand (7.0%). Such an exothermic peak has already been observed for titanium peroxo complexes [52]. Note that no weight loss with an exothermic point was observed for complex **1** (Fig. 5a), suggesting that no peroxo ligand was present. The thermal stability of the peroxo copper intermediate **2** was much higher than those of reported copper peroxo complexes [13–18]. Above 200 °C, the decomposition of organic ligands for complexes **1** and **2** began around 240 °C with exothermic peaks at 238.0 and 242.7 °C, respectively.

Resonance Raman spectra for complexes **1** and **2** in the range of 700–850 cm^{-1} and 2700–3100 cm^{-1} are shown in Figs. 6a and b, respectively. In the range of 700–850 cm^{-1}, a new peak at 805 cm^{-1} was observed for complex **2**, as shown in Fig. 6a. This peak was assigned as the intra-peroxide stretch of the bridging peroxide on the basis of its frequency. The 805 cm^{-1} O–O stretch was in the range of 800–840 cm^{-1}, which was observed for μ-1,2-*trans*-Cu^{II}–OO–Cu^{II} complexes [13,53,54] and was in the upper range of O–O stretching frequencies observed in side-on Cu^{II}–OO–Cu^{II} (around 760 cm^{-1}) [13] and $Cu^{III}(\mu_2\text{–}O)_2Cu^{III}$ (590–616 cm^{-1}) complexes [51,55] but in the down range of O–O stretching frequencies observed in copper(II) hydroperoxide species (892 cm^{-1}) [14].

Several peaks at 2861, 2907, 2932, and 2949 cm^{-1} assigned to C–H vibrations of the cyclohexane ring were observed for both complexes **1** and **2**, as shown in Fig. 6b. All

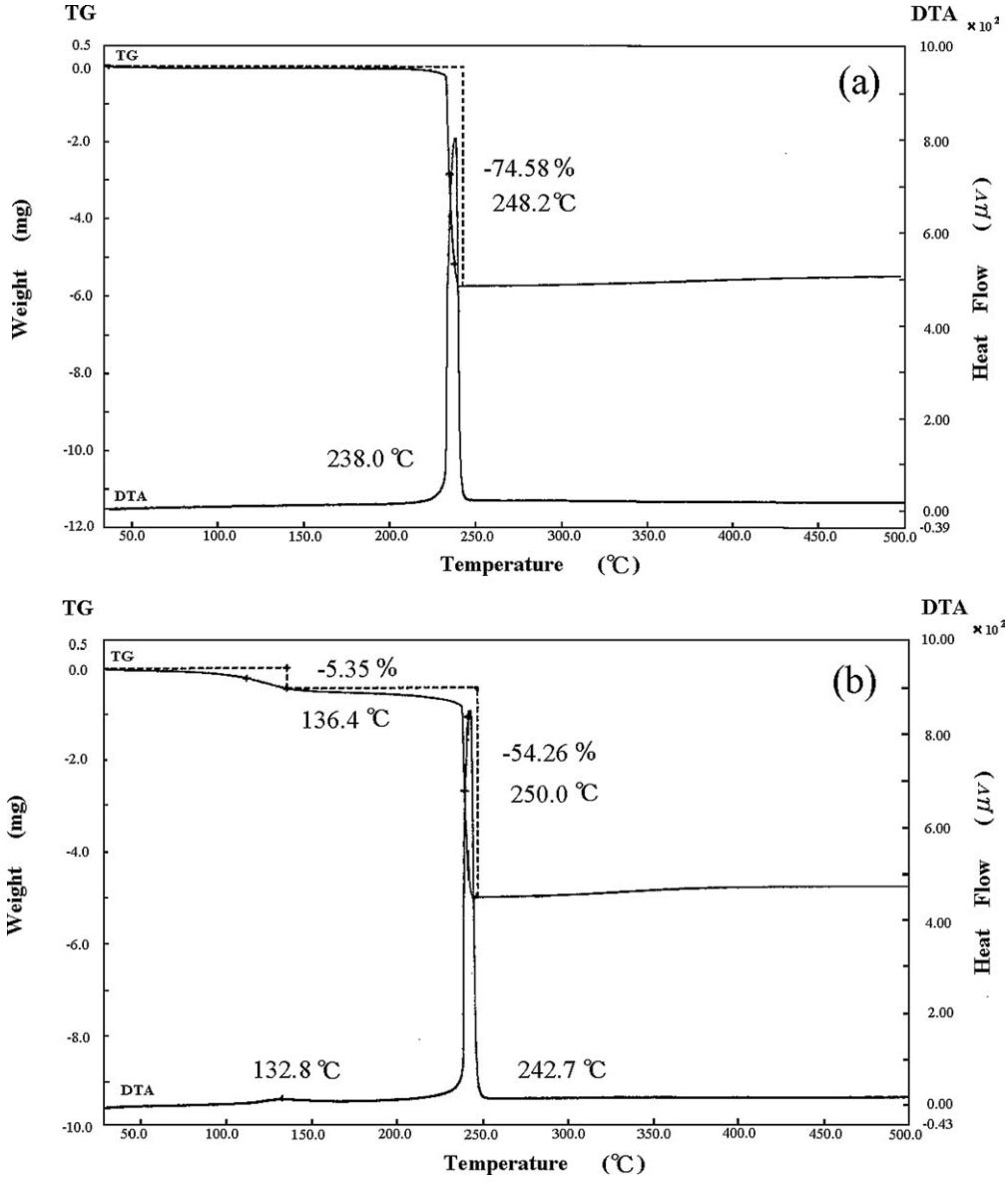

Fig. 5. TG/DTA data of (a) complex **1** and (b) complex **2**.

positions of these peaks were the same, but the relative intensities were different. This might be due to the rotation of the cyclohexane ring by intramolecular bridging of Cu–OO–Cu species between two-dimensional layers.

The diffuse reflectance (DR) UV–vis spectrum (Fig. S1a) of **1** showed two absorption bands at 384 and 655 nm due to ligand-to-metal charge transfer (CT) and *d*–*d* transition bands, respectively [9,56]. The DR UV–vis spectrum of **2** also exhibited a CT band at 385 nm and a *d*–*d* band at 665 nm (Fig. S1b). The UV–vis spectra for μ-1,2-*trans*-Cu^{II}–OO–Cu^{II} complexes, $[Cu^{II}_2(bpman)(O_2)]^{2+}$ (bpman = 2,7-bis[bis(2-pyridylmethyl)amiomethyl]-1,8-nephthyridine) [53] and $[\{LCu^{II}\}_2(O_2)]^{2+}$ (L = tris[(2-pyridyl)methyl]amine) [50], showed two new bands at 505 nm and 620 (br) nm and 525 and 590 (br) nm, respectively by the coordination of peroxo ligand to dicopper sites. In contrast, complex **2** showed only one broad band at around 665 nm, owing to the presence of an intense band of copper-carboxylate fragment. However, the position at 665 nm was shifted to a longer wavelength, suggesting the coordination of H_2O_2 to the Cu atom.

The temperature dependence of the magnetic susceptibility of complex **1** is shown in Fig. S2a. It is indicated that the effective magnetic moment μ_{eff} was 1.29 B.M. at 300 K, suggesting the presence of antiferromagnetic coupling between two copper(II) atoms in the copper center. The susceptibility of complex **1** increased with decreasing temperature until a maximum was reached at ca. 2 K, beyond which the susceptibility decreased. This showed a typical strong antiferromagnetic coupling between two copper(II) atoms in a copper center [56]. The magnetic parameters can be estimated as $g = 1.96$, $-2J = 320.4\ cm^{-1}$ emu/mol, and

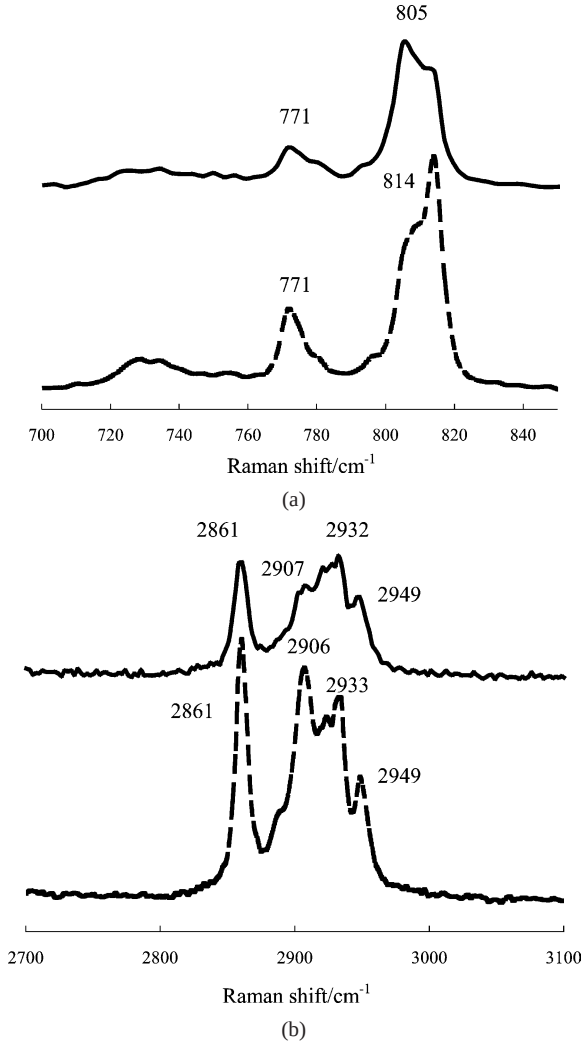

Fig. 6. Resonance Raman spectra, using an excitation wavelength of 532 nm, of complex **1** (- - -) and complex **2** (—) in the range of (a) 700–850 cm^{-1} and (b) 2700–3100 cm^{-1}.

$P = 1.4\%$ (impurity) from the best fit of the χ_A values to the Bleaney–Bowers equation [57]

$$\chi_A = Ng^2\beta^2/kT\left[(1-P)/\left(3+(-2J/kT)+\tfrac{3}{4}P\right)\right] \qquad (3)$$

where J denotes the exchange integral between copper(II) ions in binuclear copper(II) complexes. Fig. S2b also shows the temperature dependency of the magnetic susceptibility of complex **2**, in which the susceptibility increased with decreasing temperature until a maximum was reached at ca. 2 K, after which the susceptibility of **1** also decreased. The magnetic parameters can be estimated as $g = 2.01$, $-2J = 358.9\ cm^{-1}$, and $P = 0.9\%$ (impurity) from the best fit of the χ_A values to Eq. (3). This showed that there was an antiferromagnetic exchange interaction between the two copper(II) ions in **2**. Accordingly, the copper(II) centers in **2** still maintained a dinuclear copper structure, which was the same as that of as-prepared complex **1**, suggesting that complex **1** was stable toward H_2O_2, at least under the present conditions. Minor changes in the magnetic characteristics were observed for **1** with the addition of H_2O_2. This also supports the Rietveld observation that the peroxo ligand coordinated to the intramolecular Cu center to form the Cu–OO–Cu species between layers.

Both electron paramagnetic resonance (EPR) spectra for complexes **1** and **2,** which were measured at room temperature, showed EPR silent states due to strong antiferromagnetic coupling between two copper(II) atoms.

To examine the porosity of complexes **1** and **2**, Ar isotherms at 87.3 K were measured in a relative pressure (P/P_0) range from 10^{-6} to 1. These adsorption isotherms showed typical isotherms of Langmuir type, confirming the presence of micropores without mesopores. Analyses of these isotherms yielded a BET surface area of 393.9 m^2/g and 328.4 m^2/g, respectively; and both had an effective pore size of 4.9 Å (see Table 4 and Fig. 7). The porosity of complex **2** was quite high, and the surface area and pore size of **2** were almost the same as those of **1**. The absorptions of nitrogen occurred at temperatures below 200 K for both complexes, and the maximum amounts of occluded N_2 gas for **1** and **2** were, respectively, 1.27 and 1.09 mol/mol of Cu at 77.5 K (see Table 4 and Fig. S3). These results suggested that the micropore for **1** was not degraded toward H_2O_2 and not changed by the formation of Cu–OO–Cu species between layers, which is consistent with the results of the Rietveld method, as mentioned above.

Finally, to determine whether the oxidizing complex **2** is actually an active intermediate for heterogeneous oxidation catalysis, its characteristic reaction with 2-propanol was studied in a suspension of **2** in acetonitrile-d_3 in a NMR tube at 20 °C, to which 3 equivalents of 2-propanol were added. After being allowed to stand for 4 h, the solution was analyzed with a ^1H NMR spectrometer. Acetone was detected for complex **2** in the absence of H_2O_2, showing that complex **2** was actually an oxidative intermediate in the heterogeneous system.

With regard to the reaction mechanism, the results that (1) when the green color of the copper–peroxo intermediate disappeared, the reaction stopped; (2) no induction period was observed for the oxidation of 2-propanol; and (3) the obtained complex **2** was the active species suggested that the

Table 4
Maximum amount of nitrogen occluded, pore size, and surface area of microporous copper(II)-containing coordination polymers

Complexes	Amount of N_2 occluded[a]	Pore diameter (Å)	Surface area (m^2/g)
$[Cu_2^{II,II}(OOCC_6H_{10}COO)_2]\cdot H_2O$ (**1**)	1.27	4.9	393.9
$H_2[Cu_2^{II,II}(OOCC_6H_{10}COO)_2(O_2)]\cdot H_2O$ (**2**)	1.09	4.9	328.4

[a] mol/mol of copper atom.

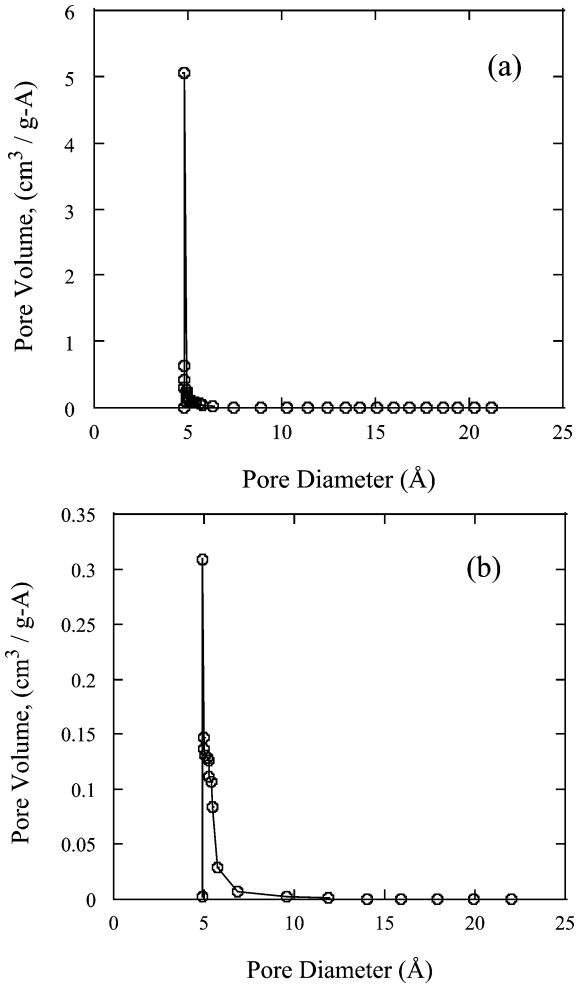

Fig. 7. Pore size distribution of (a) complex **1** and (b) complex **2**.

oxidation reaction proceeded via the formation of the copper peroxo intermediate, **2** [9]. In addition, the result that the rate for oxidation of 1-octanol was much faster than that for 2-octanol oxidation suggested that the copper-alcoholate intermediate might also be formed by the coordination of alcohol to copper centers, and the alcoholate species undergoes typical β elimination to afford the corresponding carbonyl compound and **1**, and then the cycle could be repeated [45–48].

4. Conclusions

In this paper, the results on the heterogeneous oxidations of various alcohols with H_2O_2 catalyzed by *trans*-1,4-cyclohexanedicarboxylate dinuclear copper(II) complex have shown that (1) the catalytic reactions were quite selective, with high conversions and turnover frequencies for heterogeneous oxidations of not only benzylic and secondary alcohols, but also primary alcohols with H_2O_2 via the formations of the green and brown active oxidizing intermediates; (2) the micropore structure of **1** was stable toward H_2O_2; and (3) complex **1** was reusable for heterogeneous oxidation catalysis. We have also obtained the green-colored microporous complex, $H_2[Cu_2^{II,II}(OOCC_6H_{10}COO)(O_2)] \cdot H_2O$, **2**, which was synthesized by the reaction of complex **1** with a 20-fold excess of H_2O_2 in acetonitrile and characterized by elemental analysis, magnetic susceptibility, FT-IR, TG/DTA, DR–uv, EPR, XRPD, resonance Raman, BET surface area, pore size distribution, and gas occlusion measurements, showing that (1) μ-1,2-*trans*-Cu–OO–Cu bridging between two-dimensional layers took place to form a microporous structure; (2) the peroxo ligand was stable under 132.8 °C in a solid state; (3) complex **2** had a high micropore porosity of 4.9 Å, high surface area, and high gas occlusion property, as did the as-prepared complex **1**; and (4) complex **2** was the first example of an active copper peroxo intermediate for heterogeneous oxidation catalysis.

Acknowledgments

We acknowledge Professor S. Naito (Kanagawa University) for his advice regarding catalytic reactions. This work was supported by Grant-in-Aid for Specially Promoted Research no. 15350088 from the Ministry of Education, Science, Sports and Culture of Japan. This work was also supported by a High-tech Research Center Project of the Ministry of Education, Culture, Sports, Science and Technology, Japan. CNK is grateful for the support of the Association for the Progress of New Chemistry and Grant-in-Aid for Specially Promoted Research no. 16750126 from the Ministry of Education, Science, Sports and Culture of Japan.

Supporting Information

The online version of this article contains additional supporting information.

Please visit DOI: 10.1016/j.jcat.2004.11.032.

References

[1] R.A. Sheldon, J.K. Kochi, Metal Catalyzed Oxidations of Organic Compounds, Academic Press, New York, 1981.
[2] C.L. Hill, in: A.L. Baumstark (Ed.), Advances in Oxygenated Processes, vol. 1, JAI, London, 1988, p. 1.
[3] M. Hudlucky, Oxidation in Organic Chemistry, in: ACS Monograph Series, American Chemical Society, Washington, 1990.
[4] E. Armengol, A. Corma, V. Fornés, H. Garcìa, J. Promo, Appl. Catal. A 181 (1999) 305.
[5] Z. Fu, J. Chen, D. Yin, L. Zhang, Y. Zhang, Catal. Lett. 66 (2000) 105.
[6] C.-L. Tsai, B. Chou, S. Cheng, J.-F. Lee, Appl. Catal. A 208 (2001) 279.
[7] C.R. Jacobs, S.P. Varkey, P. Ratnasamy, Micropor. Mesopor. Mater. 33 (1998) 465.
[8] L. Kevan, J.-S. Yu, Res. Chem. Intermediates 15 (1991) 67.
[9] A.O. Kuzmin, G.L. Elizarova, L.G. Matvienko, E.R. Savinova, V.N. Parmon, Mendeleev. Commun. (1998) 211.
[10] J.G. Handique, J.B. Baruah, J. Mol. Catal. A Chem. 172 (2001) 19.
[11] N. Kitajima, Y. Moro-oka, Chem. Rev. 94 (1994) 737.

[12] P.A. Vigato, S. Tamburini, Coord. Chem. Rev. 106 (1990) 25.
[13] M.J. Baldwin, D.E. Root, J.E. Pate, K. Fujisawa, N. Kitajima, E.I. Solomon, J. Am. Chem. Soc. 114 (1992) 10421.
[14] D.E. Root, M. Mahroof-Tahir, K.D. Karlin, E.I. Solomon, Inorg. Chem. 37 (1998) 4838.
[15] T. Ohta, T. Tachiyama, K. Yoshizawa, T. Yamane, T. Uchida, T. Kitagawa, Inorg. Chem. 39 (2000) 4358.
[16] N. Kitajima, T. Koda, Y. Iwata, Y. Moro-oka, J. Am. Chem. Soc. 112 (1990) 8833.
[17] E. Monzani, L. Quinti, A. Perotti, L. Casella, M. Gullotti, L. Randaccio, S. Geremia, G. Nardin, P. Faleschini, G. Tabbí, Inorg. Chem. 37 (1998) 553.
[18] E. Monzani, G. Battaini, A. Perotti, L. Casella, M. Gullotti, L. Santagostini, G. Nardin, L. Randaccio, S. Geremia, P. Zanello, G. Opromolla, Inorg. Chem. 38 (1999) 5359.
[19] H. Hayashi, S. Fujinami, S. Nagatomo, S. Ogo, M. Suzuki, A. Uehara, Y. Watanabe, T. Kitagawa, J. Am. Chem. Soc. 122 (2000) 2124.
[20] W. Mori, O. Yamauchi, Y. Nakao, A. Nakahara, Biochem. Biophys. Res. Commun. 66 (1975) 725.
[21] W. Mori, F. Inoue, K. Yoshida, H. Nakayama, S. Takamizawa, M. Kishida, Chem. Lett. (1997) 1219.
[22] T. Ohmura, W. Mori, M. Hasegawa, T. Takei, A. Yoshizawa, Chem. Lett. 32 (2003) 34.
[23] W. Mori, S. Takamizawa, in: A. Nakamura, N. Ueyama, K. Yamaguchi (Eds.), Organometallic Conjugation, vol. 1, Kodansya–Springer, Tokyo, 2000, p. 179.
[24] O.M. Yaghi, G. Li, H. Li, Nature 378 (1995) 703.
[25] L. Wang, P. Brazis, M. Rocci, C.R. Kannewurf, M.G. Kanatzidis, Chem. Mater. 10 (1998) 3298.
[26] M. Kondo, T. Yoshitomi, K. Seki, H. Matsuzaka, S. Kitagawa, Angew. Chem. Int. Ed. 36 (1998) 1725.
[27] M. Aoyagi, K. Biradha, M. Fujita, J. Am. Chem. Soc. 121 (1999) 7457.
[28] T.M. Reineke, M. Eddaoudi, M. Fehr, D. Kelley, O.M. Yaghi, J. Am. Chem. Soc. 121 (1999) 1651.
[29] H.J. Choi, T.S. Lee, M.P. Suh, Angew. Chem. Int. Ed. 38 (1999) 1405.
[30] M. Fujita, Y.J. Kwon, S. Washizu, K. Ogura, J. Am. Chem. Soc. 116 (1994) 1151.
[31] T. Sato, W. Mori, C.N. Kato, T. Ohmura, T. Sato, K. Yokoyama, S. Takamizawa, S. Naito, Chem. Lett. 32 (2003) 854.
[32] S. Naito, T. Tanibe, E. Saito, T. Miyao, W. Mori, Chem. Lett. (2001) 1178.
[33] M. Fujita, Y.J. Kwon, S. Washizu, K. Ogura, J. Am. Chem. Soc. 116 (1994) 1151.
[34] K. Seki, S. Takamizawa, W. Mori, Chem. Lett. (2001) 122.
[35] K. Seki, J. Chem. Soc. Chem. Commun. (2001) 1496.
[36] W. Mori, S. Takamizawa, J. Solid State Chem. 152 (2000) 120.
[37] W. Mori, T.C. Kobayashi, J. Kurobe, K. Amaya, Y. Narumi, T. Kumada, K. Kindo, H.A. Katori, T. Goto, N. Miura, S. Takamizawa, H. Nakayama, K. Yamaguchi, Mol. Cryst. Liq. Cryst. 306 (1997) 1.
[38] W. Mori, F. Inoue, K. Yoshida, H. Nakayama, S. Takamizawa, M. Kishita, Chem. Lett. (1997) 1219.
[39] S. Takamizawa, T. Ohmura, K. Yamaguchi, W. Mori, Mol. Cryst. Liq. Cryst. 342 (2000) 199.
[40] T. Ohmura, W. Mori, H. Hiraga, M. Ono, Y. Nishimoto, Chem. Lett. 32 (2003) 468.
[41] W. Lin, H. Ngo, in: P. Yang (Ed.), The Chemistry of Nanostructured Materials, World Scientific, London, 2003, p. 261.
[42] G. Harvath, K. Kawazoe, J. Chem. Eng. Jpn. 16 (1983) 470.
[43] G. Socrates, Infrared and Raman Characteristic Group Frequencies, third ed., Wiley, New York, 2001.
[44] W. Mori, unpublished work.
[45] G.-J. ten Brink, I.W.C.E. Arends, R.A. Sheldon, Science 287 (2000) 1636.
[46] K. Yamaguchi, N. Mizuno, Angew. Chem. Int. Ed. 41 (2002) 4538.
[47] K. Yamaguchi, N. Mizuno, Chem. Eur. J. 9 (2003) 4353.
[48] K.B. Sharpless, A. Kageyasu, K. Oshima, Tetrahedron Lett. (1976) 2503.
[49] R. Nukada, W. Mori, S. Takamizawa, M. Mikuriya, M. Handa, H. Naono, Chem. Lett. (1999) 367.
[50] R.R. Jacobson, Z. Tyeklar, A. Farooq, K.D. Karlin, S. Liu, J. Zubieta, J. Am. Chem. Soc. 110 (1988) 3690.
[51] V. Mahadevan, Z. Hou, A.P. Cole, D.E. Root, T.K. Lao, E.I. Solomon, T.D.P. Stack, J. Am. Chem. Soc. 119 (1997) 11996.
[52] G.K. Dewkar, M.D. Nikalje, I.S. Ali, A.S. Paraskar, H.S. Japtap, A. Sudalai, Angew. Chem. Int. Ed. 40 (2001) 405.
[53] C. He, J.L. DuBois, B. Hedman, K.O. Hodgson, S.J. Lippard, Angew. Chem. Int. Ed. 40 (2001) 1484.
[54] K.D. Karlin, R.W. Cruse, Y. Gultneh, J.C. Hayes, J. Zubieta, J. Am. Chem. Soc. 106 (1984) 3372.
[55] H. Hayashi, S. Fujinami, S. Nagatomo, S. Ogo, M. Suzuki, A. Uehara, Y. Watanabe, T. Kitagawa, J. Am. Chem. Soc. 122 (2000) 2124.
[56] W. Mori, T. Sakurai, A. Nakahara, Inorg. Chim. Acta. 132 (1987) 247.
[57] B. Bleaney, K.D. Bowers, Proc. R. Soc. London, Ser. A 214 (1952) 451.